Gaussian Process Regression (GPR)-based missing data imputation and its uses for bridge structural health monitoring

Dalmasso *et al.*
Advances in Bridge Engineering (2025) 6:23
https://doi.org/10.1186/s43251-025-00169-1

Advances in
Bridge Engineering

ORIGINAL INNOVATION

Open Access

Gaussian Process Regression (GPR)-based missing data imputation and its uses for bridge structural health monitoring

Matteo Dalmasso[1], Marco Civera[1*], Valerio De Biagi[1] and Bernardino Chiaia[1]

*Correspondence:
marco.civera@polito.it

[1] Department of Structural, Geotechnical and Building Engineering, Politecnico di Torino, Corso Duca degli Abruzzi, 24, Turin 10129, Italy

Abstract

Structural health monitoring (SHM) apparatuses rely on continuous measurement and analysis to assess the safety condition of a target system. However, in field applications, the SHM framework is often hampered by practical issues. Among them, missing data in recorded time series is arguably the most common and most disruptive challenge that can arise. Therefore, imputing missing values is necessary to maintain the integrity and utility of the SHM data. This research work investigates the use of Gaussian Process Regression (GPR) for imputing missing data in ordered time series. In particular, this approach is here proposed and tested for Vibration-Based Monitoring (VBM) and ambient monitoring, with applications to modal parameters and air temperature. Both punctual missing-at-random (MAR) and prolonged missing-not-at-random (MNAR) gaps in the time histories of recorded natural frequencies are analysed. The performance of the proposed GPR-based approach is evaluated on real-life data from field tests on a well-known case study, the KW51 rail bridge. The method is first tested to actual missing values in the dataset. Then, the accuracy is tested using artificially removed data, and the imputed values are compared to the ground truth (i.e., the actual measured data). In the first case, the results show that the complete time series are deemed qualitatively similar to what would be expected by an expert user. The outcomes of the second part quantitatively demonstrate that GPR can accurately impute missing data in modal parameter time series, preserving the statistical properties of the data.

1 Introduction: the missing data problem in SHM

The missing data problem affects several studies in a variety of fields, such as clinical trials, sociological surveys, the collection of physical measures and engineering data (Luo 2022). In all these specific applications, missing data hamper the overall interpretation of the system under observation. Furthermore, for data-driven predictive modelling, where the physical principles are only partially known, the lack of available measurements can induce wrong outcomes in Machine Learning (ML)-based regression and classification (Emmanuel et al. 2021). Indeed, the occurrence of missing data introduces a certain level of uncertainty; if these analyses are mishandled, the results could be biased and ineffective (Mason et al. 2010a; Ma & Chen, 2018). To address this problem, there are generally

two possible approaches: ad-hoc approaches or statistically principled methods. The main advantage of the former is their simplicity; on the other hand, they lack generalisation and can lead to bias and loss in precision. In this sense, imprecise missing data imputation can affect data-driven damage assessment even more negatively (Shadbahr et al. 2023). On the other hand, the latter group of algorithms is generally preferable, as they incorporate information from the observed data and the uncertainty arising from the missing data through assumptions regarding the missing data mechanisms (Mason A. et al. 2010b). A more detailed and multidisciplinary discussion about all these aspects can be found in (Emmanuel et al. 2021) and (Lin & Tsai 2020).

One of the main statistically principled methods used is the fully Bayesian (FB) framework. In a single step, this method addresses missing data by applying an imputation model to create multiple imputed datasets, fitting the analysis model, and calculating pooled estimates. Additionally, it can directly and simultaneously extract estimates from the posterior distributions of the parameters and missing variables (Erler et al. 2016). With the Bayesian approach, it is possible to account for the uncertainties arising from missing data when inferring from incomplete datasets. The missing data are deemed random variables by specifying prior parameters and the distribution of the missing covariate. The posterior distribution can then be obtained (Daniels & Hogan 2008; Ibrahim et al. 2005) by incorporating informative priors and extra data; this way, Bayesian methods can provide better and more dependable results, even with small sample sizes.

In the civil engineering field, particularly in the context of Structural Health Monitoring (SHM), dealing with missing data is, unfortunately, very common. Indeed, this field is based on using sensors that measure static and/or dynamic quantities on monitored structures or infrastructures, subsequently to study them and define the condition of the construction investigated. Often, the sensors do not function perfectly during the analysis of measured quantities, so researchers must deal with missing data. Depending on the type of malfunction, the missing data can have two patterns. The first pattern consists of single random missing data points; in this case, the sensors occasionally fail to acquire data. This instance is known as the missing-at-random (MAR) scenario. The second pattern involves a series of consecutive missing data points; in this case, the sensor malfunction is persistent. This case is often referred to as a missing-not-at-random (MNAR) scenario.

The method used in this paper is Gaussian Process Regression (GPR), which, as mentioned earlier, is a Bayesian approach. More information about this method, including its basics and functioning, will be described in the next Section. In the civil engineering field, several publications have been published about the use of the above-mentioned method. For instance, in the geotechnical branch, GPR has been used to formulate models to forecast Finland's soft-sensitive clays' undrained shear strength, being able to associate an equation that represents the undrained shear strength of clays of Finland from laboratory and in situ data (Assolie 2024). It was adopted to prognosticate the Californian Bearing Ratio (CBR) values, creating an accurate model that embraces several soil characteristics (i.e. distribution, plasticity, linear shrinkage, stabilising additives) (Wu et al. 2024). The algorithm was used to create a model to predict the effective stress parameters of unsaturated soil (Samui & Jagan 2013). Another application of GPR is related to foreseeing the load-bearing capacity of piles, using the actual pile driving records both to train the model and to validate

the results of the model (Pal & Deswal 2010). Finally, it is used to define a methodology for the prediction of the spatial distribution and depth of the bedrock layer over a large area, employing the data of a limited number of borings (Tsuda et al. 2023).

The GPR is also used in the process of mix design; for example, it defines a model of the compressive strength of high-performance concrete (HPC), trying to define the relationship between the compressive strength and the constituent of the HPC mixture (Hoang et al. 2016). In another study, the shear strength of recycled beams has been predicted based on the characteristics of recycled aggregates, concrete properties, longitudinal and transverse reinforcement ratios, and the geometrical ratio of the beam. The experimental studies have been used as the input dataset (Omidinasab et al. 2023).

Further to this paper's topic, the GPR has also been utilised in the field of Structural Health Monitoring (SHM); for instance, it has been applied to the well-known, versatile, and robust framework of system identification called NARX (Nonlinear Auto-Regressive with eXogenous inputs). The framework is established on a nonlinear discrete-time representation. By merging the NARX framework with the GPR, an analytical derivation of Higher-Order Frequency Response Functions (HFRFs) was obtained, creating a test for nonlinearity that can detect system nonlinearity (Worden et al. 2018). The theory has been expanded by converting the prediction limits in the time domain on the bounds of HFRFs (Worden et al. 2017). Additionally, the GPR estimation has been used to define the existence and the position of manufacturing imperfections in pultruded glass fibre-reinforced polymer profiles. In this application, the GPR has been combined with the Bayesian-based Recursive Partitioning (also known as Treed Gaussian Process). The results of the estimation have been compared with the numerical results obtained with Finite Element Models (FEMs) (Civera et al. 2020). The same method was used to locate the cracks in beams identifying singularities in mode shape curvatures (Civera et al. 2017). Further employment of GPR is the inferring of infrastructure components defining their condition state, considering stressors located in different positions (Pozzi & Wang 2018).

An evolution of the GPR, called the physics-informed Gaussian process regression (Pi-GPR) was employed to predict the fatigue life of welded joints, integrating the physical features of fatigue fracture mechanics and thus reducing the dependency on the model from an extensive experimental dataset (Kim et al. 2024).

The remainder of this paper is organised as follows. In Section 2, a brief description of the GPR theory is presented; thereafter, the algorithm used is outlined, defining the procedure followed to obtain the dataset, its analysis, and post-processing. In Section 3, the case study is introduced, describing the bridge and the monitoring system installed on it. The Results of all the cases analysed are presented and discussed in Section 4. The methodology is also compared to other imputation methods (Subsection 4.1.1) and validated for applications to ambient data monitoring (Subsection 4.1.2). Finally, the Conclusions (Section 5) complete this paper.

2 Methodology: the Gaussian process regression

GPR can be considered a generalisation of the Gaussian Distribution (GD). GD is defined over vectors and is completely defined by the mean vector and the covariance matrix. Meanwhile, the GPR is outlined over function and is completely defined by its mean function $m(x)$ and covariance function $k(x, x')$ (Rasmussen 2004). GPR

defines the probability distribution over functions, computing the mean and the variance. The mean represents the maximum likelihood, while the variance is a measure of confidence. As a nonlinear, nonparametric kernel-based probabilistic model, GPR is highly effective for interpolating data points dispersed in a high-dimensional input space. A key strength of the GPR is to predict the value of a response variable y_{new}, using the training dataset $\{(x_i, y_i) i = 1,2,\ldots,n\}$ and the new input data vector x_{new}.

In the GPR model, the response is defined through explicit basis functions h, projecting inputs into a p-dimensional feature space. The latent variables $f(x_i)$, where $i = 1,2,\ldots,n$, capture the smoothness of the response.

Equation 1 represents a linear regression model, where $\varepsilon \sim N(0, \sigma^2)$, with β and σ^2 are estimated from the data. Considering the GPR model, its mathematical expression is outlined in Eq. 2. In this equation, $h(x)$ denotes the set of basic functions that transform the feature vector $x \in R^d$ into a new feature vector $h(x) \in R^p$. The coefficient vector β is a p-by-1 vector of basis function weights, while $f(x) \sim GP(0, k(x, x'))$, $f(x)$ describes a zero mean Gaussian Process with covariance function $k(x, x')$.

$$y = x^T \beta + \varepsilon \tag{1}$$

$$GP = h(x)^T \beta + f(x) \tag{2}$$

As modelled in Eq. 3, the response relies on the latent variable $f(x_i)$ introduced for each observation x_i, making the GPR model nonparametric and probabilistic (1994–2024 The MathWorks n.d.).

$$P(y_i | f(x_i), x_i) \sim N\left(y_i | h(x_i)^T \beta + f(x_i), \sigma^2\right) \tag{3}$$

The covariance function $k(x, x')$ is typically parameterised by a set of kernel parameters or hyperparameters, denoted as θ. The kernel function plays a crucial role in the model's capability to generalize, choosing an appropriate function for a specific task is essential. Some kernel functions are well established and standardly used, while others, more peculiar alternatives, can be customised for specific uses. Moreover, the performances of the process heavily depend on the hyperparameters optimisation (Jie Wang 2024).

The GPR is extensively used in Machine Learning (ML) applications thanks to the capability to quantify uncertainty over predictions and their representation flexibility (Jie Wang 2024). In particular, GPR is a non-parametric, probabilistic supervised Machine Learning (ML) technique that shines in regression and classification applications. By utilising prior knowledge (kernels), it identifies repeating patterns in the data, generates predictions and provides uncertainty estimation for those predictions. Unlike other regression methods (i.e., linear or polynomial), which rely on a definite number of parameters, GPR, being non-parametric, dynamically adapts its complexity.

The proposed GPR-based imputation method offers several advantages for SHM applications. First and foremost, as is well known, it makes no assumptions about the underlying distribution of the data. Secondly, it can handle non-linear and non-stationary time series. The probabilistic (Bayesian) nature of GPR also provides uncertainty estimates for the imputed values. As will be shown in the Results, this is of the utmost importance, as

for each punctual missing data point, or even more importantly, for each missing range of data points, the provided output is not a deterministic value but rather a probability distribution.

By maintaining complete and accurate modal parameter time series, GPR imputation enables reliable damage detection and condition assessment using advanced SHM techniques. The method applies to a wide range of SHM applications beyond bridges, such as monitoring of residential buildings, offshore structures, and wind turbines.

The algorithm is built on Matlab™, a program for numerical calculation and statistical analysis, with the GPML software package (Rasmussen & De 2010) as an additional toolbox. The code comprises sections that enable the following: loading data from the repository, selecting and manipulating the data, applying the GPR, and, finally, performing the post-processing phase. In the following, a more detailed description of each step is provided:

- *Data loading*: The data accessed comes from the monitoring campaign on the KW51 rail bridge, located in Belgium. The loaded files are the time history of the identified modal characteristics. For every time step (i.e. one hour), the MATLAB file contains a struct with an averaged value of identified natural frequencies in Hz, identified modal dumping ratio in %, identified displacement mode shapes, environmental data in SI unit, the UTC time vector in serial data number format and the corresponding label vectors. Whenever a value is not specified for a given time step, "NaN" is inserted in place of the missing data point.
- *Data processing*: The natural frequency values have been normalised, specifically using the conventional min–max normalisation formula:

$$z = \frac{f - \min(f)}{\max(f) - \min(f)} \tag{4}$$

  which reduces the range of variation of the raw identified natural frequencies f (in Hz) to z values defined in the range between 0 and 1, while the temperature data remained unchanged. Finally, both data types were subsampled, retaining one value out of ten, solely to expedite the subsequent analyses. Further data manipulations have been applied to the subset, and they will be presented in the dedicated sections that follow.

- *Application of GPR:* With the GPML package, it is possible to apply GPR for posterior inference, learning hyperparameters, computing the marginal likelihood, and making predictions. The function requires a hyperparameter struct, an inference method, a mean function, a covariance function, a likelihood function, training inputs, training targets, and optional test cases as inputs. In this case, the Squared Exponential covariance function and the Gaussian likelihood have been chosen as covariance and likelihood functions, respectively. The hyperparameters (mean, covariance, and likelihood) have been initialised. Notably, in this application, the mean function does not have a hyperparameter set. The Exponential covariance function has the "log of the length-scale" and the "log of the signal standard deviation" hyperparameters to be set, and the Gaussian likelihood has the "log of the noise standard deviation" as a

Fig. 1 Google earth view of the KW51 railway bridge

hyperparameter. These are set as follows: the length scale and signal standard deviation are initialised to 1, and the noise standard deviation is initially set to 0.37. Then, the hyperparameters are optimised by employing the log marginal likelihood (Rasmussen & Nickisch 2020).

- *Post-processing phase:* The outcome is the GPR prediction results, involving both the mean function and the confidence interval predicted by the GPR. Additionally, as shown in the Results, the statistical analysis of the prediction performance will be illustrated using histograms.

3 Field case study: the KW51 railway bridge

Civil infrastructures are inherently at risk of structural damage due to harsh environmental conditions, exceptional loads, or even just regular wear and tear. Road and rail bridges, in particular, can suffer damage due to a variety of causes, such as e.g. material degradation, fires (Faruqi et al. 2012), or vehicle impacts (Roy et al. 2021). Hence, their continuous monitoring is of paramount importance for the safeguarding of human lives.

In this context, this study primarily utilises field data from the KW51 railway bridge, obtained from an extensive monitoring campaign, as a case study for experimental validation.

This rail bridge (Fig. 1) is a steel-made railway bridge of the bowstring type, measuring 115 m in length and 12.4 m in width. It was opened in 2003. The bridge is located in Leuven, Belgium, at the coordinates 50.9004°N and 4.7066°E. Crossing the Leuven-Mechelen channel, it belongs to railway line L36 N, connecting Leuven and Brussels. The railway consists of two ballasted, electrified curved tracks, with a curve radius of 1,125 m for track A and 1,121 m for track B, on which a maximum travel speed is 160 km/h.

Four pot bearings support the bridge. At the bridge end in the Brussels direction, the longitudinal motion is fixed; instead, in the Leuven direction, the longitudinal movement is allowed. Notably, at the intersection with the arches and bridge deck, a steel box was welded over the original bolted connection for every diagonal. Since October 2, 2018, it has been subjected to a monitoring campaign. The instrumentation of the bridge was completed in three phases. In October 2018, the installation of accelerometers on the bridge deck was completed, along with strain gauges on the bridge deck and the diagonals connecting the bridge deck to the arches, as well as gauges on the rails. Additionally, a thermocouple was installed below the bridge deck, and a relative humidity (RH) sensor was placed. The second phase involved setting up accelerometers

Table 1 Brief description of the position and the model of the sensor installed on the KW51 rail bridge

Type of sensor	Location(s)	Brief description
Uniaxial Accelerometers	- 6 installed on the bridge deck - 6 installed on the arches	Type: PCB 393B04 with a sensitivity of about 1,000 mV/g.
Uniaxial Strain Gauges	- 8 installed on the bridge deck - 4 installed on diagonals connecting the bridge deck and the arches	Type: Micro-Measurements CEA-06-250UN-350, a single strain-sensitive element with nominal electrical resistance RG=350 Ω.
Rosette Strain Gauges	- 4 installed on the rails	Type: Micro-Measurements CEA-06-250UR-350, three strain-sensitive elements (+ 45°, 0°, and − 45°), each having a nominal resistance RG=350 Ω.
Laser-Based Displacement Sensors	- 2 installed at the bearings in the Leuven direction	Type: Welotec OWLL 8025 AD S1, operating in a range between 50 and 250 mm at a resolution of 6.3 µm.
Temperature Measurements	- Installed below the steel surface of the bridge deck	Type: Labfacility type T thermocouple with a wire length of 2 m.
Relative Humidity	- Installed near the thermocouple	Type: HM1500LF RH transducer with a sensitivity of 25.68 mV/%.

on the arches in September 2019, followed by the installation of displacement sensors at the bearings of the bridge in October 2019 (Phase 3). The complete sensing apparatus is summarised in Table 1. A full description of the sensor location and further details can be found in (Maes & Lombaert 2021). Importantly, the issue of missing data points, discussed here, is inherently linked to the deployed sensing devices and pieces of hardware. However, despite precautions at the hardware level, such as redundant sensors, as well as robust and wideband data transmission protocols, MAR and MNAR data points are inescapable in real-life applications. Any specific field implementation will have its own challenges, which can only partially be mitigated with hardware-only adjustments, highlighting the need for reliable software-based countermeasures.

From May 15 to September 27, the rail bridge underwent retrofitting, strengthening the connections between the diagonals and the arches, as well as the bridge deck, to address a construction flaw detected during maintenance checks. This retrofitting, while not a true damage, is interesting as it presents a structural change introduced during the monitoring period. As it will be clear in the time series reported and discussed in the next Section, this results in three phases: before, during, and after the retrofitting work. This returns a non-stationary time series of data, which, therefore, makes the data analysis more complex and interesting, providing a compelling case study for validating the proposed missing data imputation technique.

Thus, the data originate from the dataset collected during the monitoring campaign on the previously described bridge. The study focuses on the identified modal characteristics, including natural frequencies, damping ratios, and mode shapes, obtained from the processed acceleration measurements taken on the bridge deck and arches. The processed acceleration signal was decimated and then pre-processed using a lowpass filter. Specifically, an eighth-order Chebyshev Type I lowpass filter with a cutoff frequency of 16.5 Hz and a 0.05 dB peak-to-peak ripple in the passband was applied. To eliminate phase distortion, the filter was applied in both the forward and reverse directions. After

filtering, the signals were resampled at a rate of 41.3 Hz. The signal obtained is processed using the covariance-driven stochastic subspace identification (SSI-cov/ref) algorithm. Fourteen different modes are identified; nevertheless, no one of the modes is identified at all times, as at least a certain number of hours are missing for each identified mode. For a complete description of the processing algorithm adopted to obtain the identified modal characteristics, check the original paper of (Maes & Lombaert 2021). For brevity, only the analysis carried out on the first identified mode is reported here.

The scientific literature reports several studies above this bridge; for instance, one study involving the feasibility of an SHM system, which relies on the natural frequencies (Maes et al. 2022), the analysis of the pot bearing with its nonlinear behaviour (van de Velde et al. 2023), a continuous dynamic strain monitoring of the bridge led to the definition of the ten natural frequencies, and strain mode shapes are defined automatically employing operational strain time histories (Anastasopoulos et al. 2023), and a classification algorithm for the structural states (before, during and after retrofitting) of the bridge (Al-Ghalib & Mahmoud 2023).

4 Results

In this chapter, the GPR results for the three investigated cases are presented. The first case (Case 0) considers the complete sub-set as described in Section 2. Additionally, to evaluate the robustness of the method, the performance of the GPR is compared with that of other uncertainty estimation methods, including mean imputation and linear regression. Furthermore, the same process is applied to a different dataset, environmental monitoring data, to assess its adaptability.

The other two cases are derived from the same initial dataset with intentionally omitted data points to simulate disruptions in data recording. The missing data points are manually removed, erasing the data according to one of the following two patterns: either one-fourth of the data are randomly erased, to emulate an MAR scenario (Case 1) or n consecutive data points are removed, simulating MNAR occurrences. The number of omitted data points differs for each subcase studied, allowing for additional monitoring of the GPR performance. These additional subcases have been named Cases 2.a, 2.b, 2.c, and 2.d, respectively.

The removal process aims to mimic the case of sensor(s) malfunction that causes missing data points along the recorded signal. The malfunction can be singular and repeated over time, as depicted in Case 1, or continuous for a certain period, as represented in the several variants of Case 2, until the sensor is restarted, repaired, or replaced.

Both the results are shown by means of a graphical representation, in which the prediction obtained with the GPR in terms of mean and standard deviation, corresponding to the 5th and 95th percentile, and the training dataset are depicted. This representation provides a clear understanding of the precision and accuracy of the GPR at a glance. Additionally, in Cases 1 and 2 in the same graph, in addition to the results obtained studying that particular case, the results of the prediction of Case 0 are added. In doing so, the results of Case 0 serve as a reference for comparing the prediction obtained in the case of missing data points.

The time series plot is intended here to showcase the qualitative correlation between the algorithm's results and the measured data. On the other hand, as an additional tool

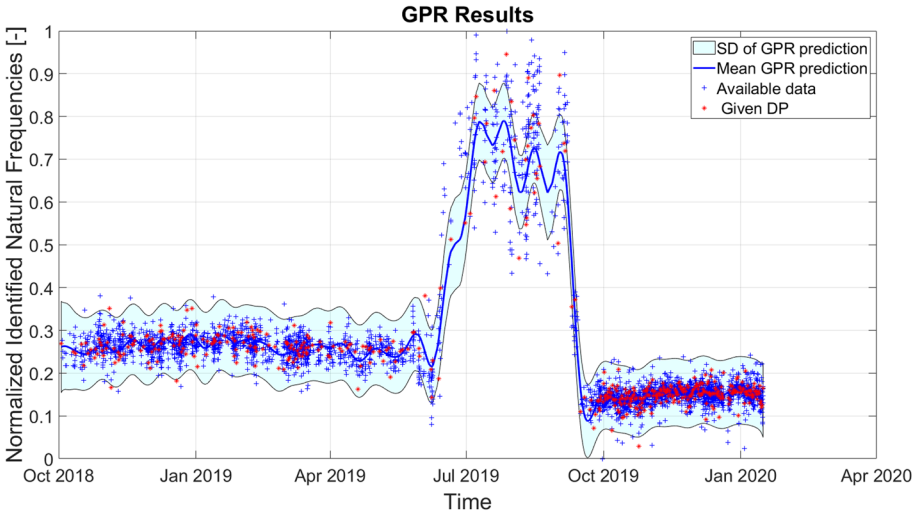

Fig. 2 Representation of the GPR prediction of Case 0. The blue line represents the mean predicted value, the light blue area indicates the confidence interval bounded by the 5th and 95th percentiles, the red stars denote the training data points (DP), and the blue crosses represent the test data points. The three phases (before, during, and after the retrofitting works) are clearly visible before and after the two dates: May 15, 2019, and September 27, 2019

to evaluate the prediction effectiveness, a histogram is employed to report a quantitative correlation, explicated through the percentage difference between the predicted GPR value and the actual one.

In the following subchapters, the results obtained in Case 0 are initially presented, as this case serves as a benchmark. Then, Cases 1 and 2, along with their subcases a, b, c, and d, are discussed.

4.1 Results of Case 0

As mentioned, Case 0, which will be used hereinafter as the benchmark, was obtained by considering 1 out of every 10 data points available in the complete dataset. The remaining ones were thus used for validation. More accurately, Case 0 is trained on a dataset of 476 identified natural frequencies. Based on this training dataset, the GPR must predict the value of natural frequencies in terms of the mean and standard deviation of all points belonging to the remaining available dataset. The results of the GPR prediction are depicted in Fig. 2.

Importantly, due to the aforementioned retrofitting works, the identified natural frequencies have three clearly defined phases: before, during, and after retrofitting. As discussed in the previous Section, that makes this dataset non-stationary and, therefore, particularly compelling to analyse for vibration-based continuous monitoring purposes.

It is clearly noticeable that the overall performance of the GPR is outstanding. The process can define a function and an interval of confidence that contains most of the data. As is easily imaginable, better results are obtained when the identified natural frequencies are more stable, approximately spanning the periods from October 2018 to May 2019 and from October 2019 to January 2020; in this case, the function and the interval of confidence contain practically all the data points. The prediction performances fall when the data are more variable. A more accurate analysis of the

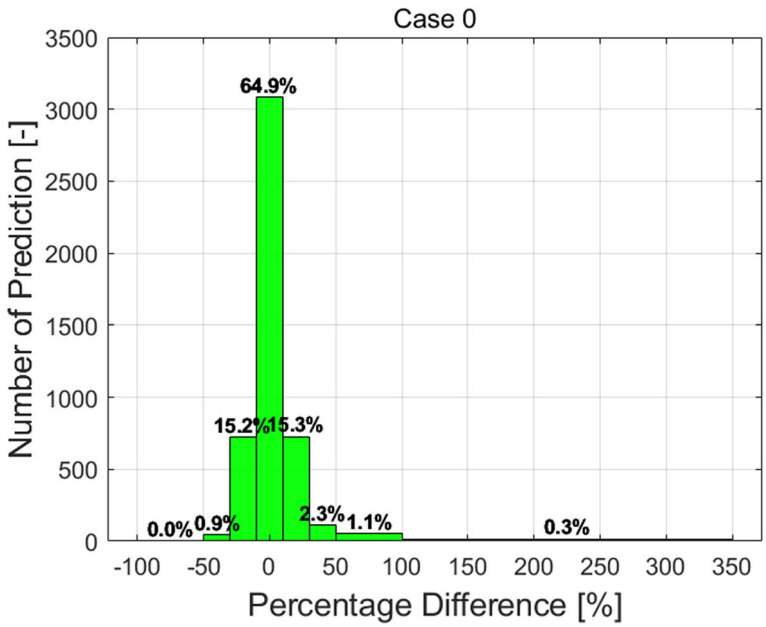

Fig. 3 Histogram representation of the percentage difference between the value of predicted frequencies and the value of corresponding identified natural frequencies (Case 0)

prediction performances obtained by applying the GPR is depicted in Fig. 3. For every time instant, the percentage difference has been calculated by subtracting the predicted GPR mean value from the corresponding actual value and then dividing the result by this known target value. The results show that in 64.9% of the cases (corresponding approximately to 3,100 predictions), the prediction error is very limited; in fact, it differs by no more than ±10% from the actual target frequency. Furthermore, in approximately 15.2% and 15.3% of cases (approximately 700 predictions), the percentage difference between the prediction and the actual value is bounded, respectively, within the ranges of −30% to −10% and +10% to +30%. Altogether, that means that in 98.6% of the cases, the percentage difference is bounded between ±50%. If one considers the classic 3-σ (99.73%) confidence interval for damage detection-see e.g. (Civera & Surace 2021)-all these imputed data points will fall largely within the bounds of the 'normal' structural behaviour, thus not triggering any false alarm.

Since this case is trained on the most comprehensive dataset, i.e., without additionally removed data points, it has been considered the benchmark results to be met for the analysis of Cases 1 and 2.

4.1.1 Comparison with other imputation methods

To better understand the effectiveness of the GPR prediction, this subsection tests other, more conventional uncertainty estimation methods; their results are then directly compared with those obtained by applying GPR.

In particular, mean imputation and linear regression are considered viable alternatives for missing data imputation. In the first case, the algorithm replaces missing values with the mean of all the non-missing values in the time series. Assuming a GD, this is identical to performing median and mode imputation. In the second case,

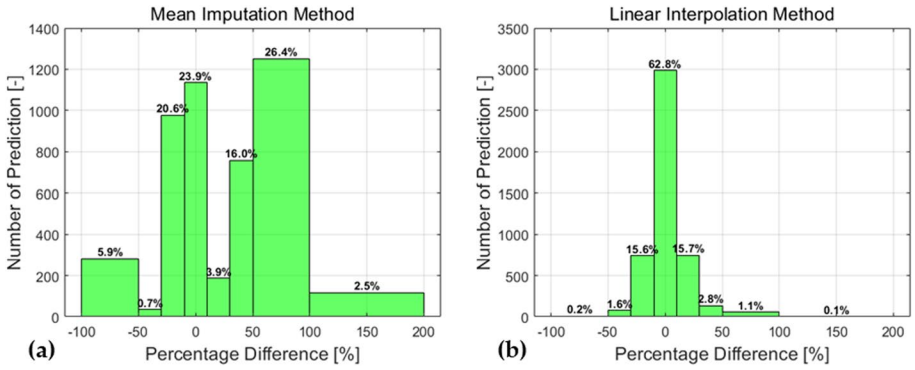

Fig. 4 Histogram representation of the percentage difference between the value obtained applying the mean imputation method (**a**) and with linear interpolation method (**b**), with the corresponding identified natural frequencies

missing data points are replaced with a linear interpolation between the last previous and the first following non-missing values. Other simpler approaches, such as forward fill and backward fill (where, respectively, the missing data points are replaced by the last available or the next available non-missing value), were also tested; the results are not reported here for brevity, as they were significantly worse than these two other options.

The same initial dataset, Case 0, composed of 476 identified natural frequencies, was provided as input to both methods. As output, it was required to estimate the natural frequencies for every time instant. The plot of estimated natural frequencies in time is omitted for the sake of brevity. To better compare the performances, only the histograms showing the quantitative correlation are shown in Fig. 4.

The mean imputation method exhibits poor performance, as illustrated in Fig. 4a. Indeed, substituting the missing values with the mean obtained from the available ones is an oversimplified, yet common, method that shows all of its limitations in terms of accuracy when dealing with non-stationary data. On the other hand, considering the linear interpolation method (Fig. 4b), the results are significantly more reliable and comparable to the GPR prediction. Indeed, in 98.5% of the cases, the percentage difference between the estimated frequency and the actual value is bounded between $\pm 50\%$. However, the primary limitation of linear interpolation is its inability to account for the probability distribution when predicting the missing data points. As shown in Fig. 5, this method can predict points that fall outside of the confidence interval defined by the GPR, placing data in low-probability areas. This drawback can be exacerbated in cases where several consecutive MNAR data points occur.

4.1.2 Application to environmental monitoring data

It is important to remark that not only damage (as a local source of reduced stiffness and/or nonlinearities) but also other factors, such as Environmental and Operational Variabilities (EOVs (Sohn 2007)), affect the vibrational response of a monitored structure. These EOVs are of paramount importance in SHM since these confounding influences severely affect the damage detection capabilities of the more accurate methodologies, as

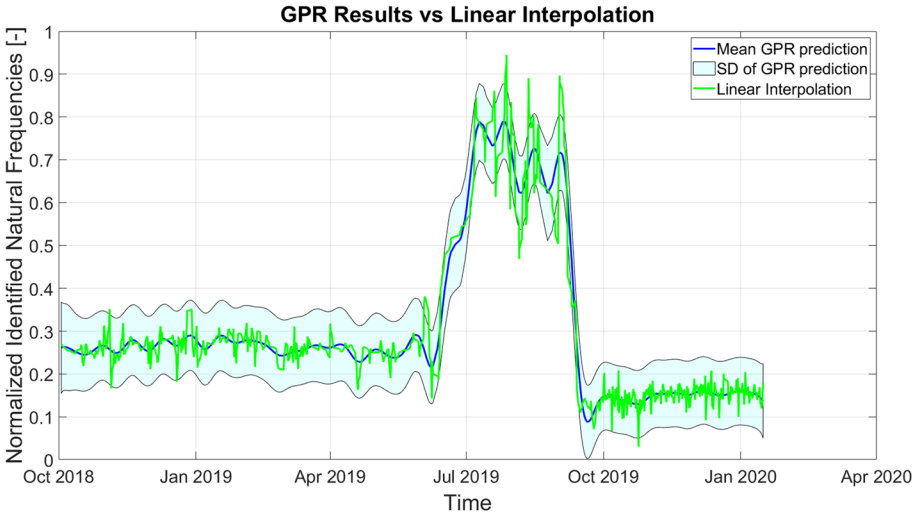

Fig. 5 Comparison in time of normalised identified natural frequencies predicted with GPR (Case 0) and with linear interpolation

they induce damage-unrelated anomalies resulting in misidentifications and false alarms (Cross et al. 2011, 2012).

In this regard, the GPR algorithm, proposed here for missing data imputation and validated on time series of identified natural frequencies, can also be applied to other types of monitored data. To this aim, it is also tested on temperature readings from the same case study. In this case, the recorded temperatures, obtained following the same data acquisition process as described in Case 0, are used as input data to the GPR algorithm. Unlike the natural frequency time histories, which exhibit clear non-stationarity corresponding to the three phases before, during, and after retrofitting works, this dataset shows that temperature variations occur with both daily and seasonal fluctuations, but without any discontinuities in these trends. Figure 6 illustrates the results of the GPR prediction.

The overall performance is good, successfully capturing the daily and seasonal temperature variation. More specifically, the predictions are more accurate in data-dense regions and less reliable in data-scarce areas, such as between May 2019 and September 2019. Histogram analysis (Fig. 7a) reveals that the prediction accuracy is lower compared to Case 0. According to the results, 30.6% of predictions (about 1,300) differ from the actual identified frequency by $\pm 10\%$. Additionally, 26.7% and 16.1% of cases exhibit percentage differences in the ranges $(-30\%, -10\%)$ and $(+10\%, +30\%)$, respectively. Collectively, 87.3% of predictions remain within a percentage difference of $\pm 50\%$. The performance deterioration is clearly due to daily temperature variation, where fluctuations of several degrees Celsius can occur within a single day. That is to say, the data values change more frequently and more rapidly, making accurate predictions more difficult and thus slightly less reliable. However, it should be stated that, even in this case, very few data points exceed the 3-σ alarm threshold.

Finally, the effectiveness of the prediction is further shown by a graph comparing the normalised identified natural frequencies and these temperature measures, which correspond to Case 0. GPR estimates (in blue) are superimposed on the target values (in

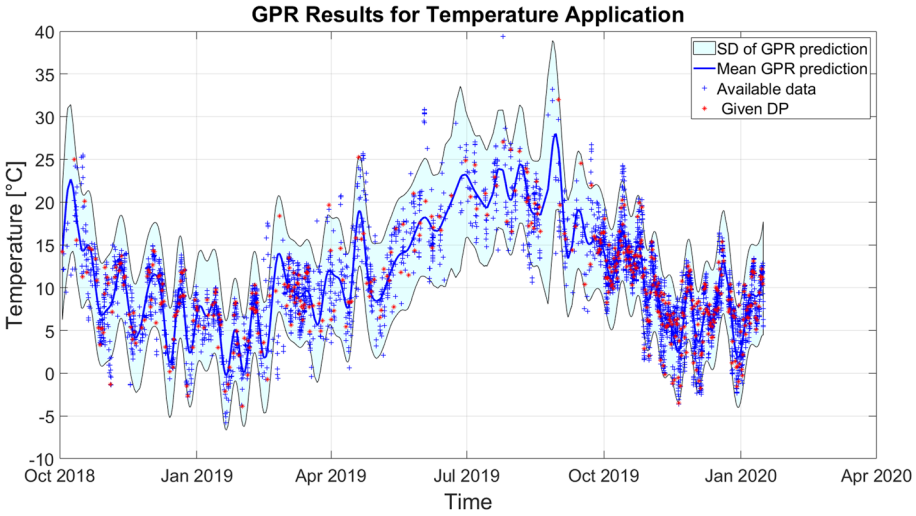

Fig. 6 Representation of the GPR prediction in the case of temperature application. The blue line represents the mean predicted value, the light blue area indicates the confidence interval bounded by the 5th and 95th percentiles, the red stars denote the training data points (DP), and the blue crosses represent the test data points

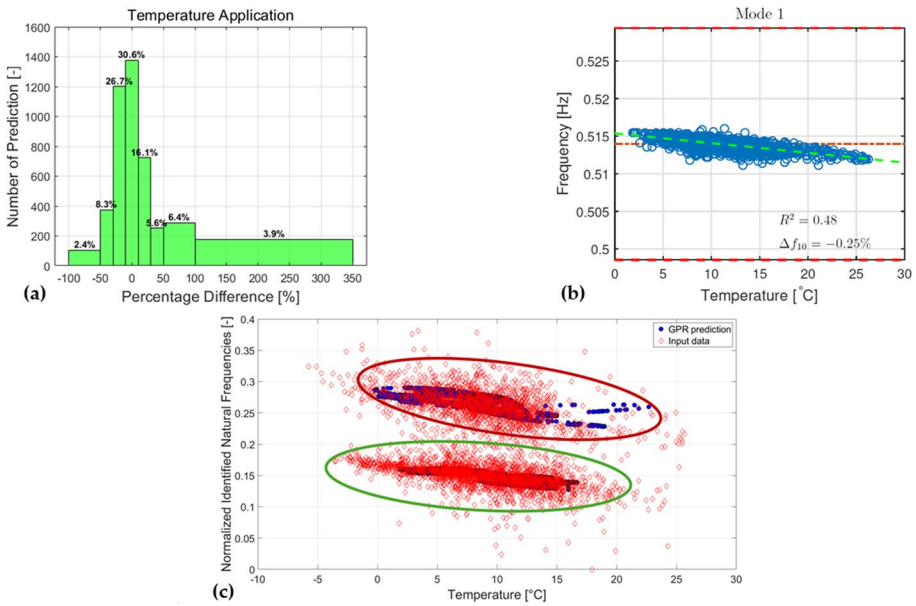

Fig. 7 **a** Histogram representation of the percentage difference between the value of predicted temperature and the value of corresponding actual temperature. **b** Expected influence of temperature on the non-normalised first frequency before retrofitting, according to (Anastasopoulos 2020). **c** Plot showing temperature versus normalised identified natural frequency. Red diamonds: actual data. Blue circles: corresponding predicted values. Two key areas are highlighted: post-retrofitting data, circled in green, and pre-retrofit data, circled in red

red). As illustrated in Fig. 7c, two clusters are identified: post-retrofitting (encircled in green) and pre-retrofitting (circled in red). The fewer data points corresponding to the retrofitting phase are omitted, as they were highly scattered due to the high variability of the identified frequencies, most likely caused by the retrofitting operations. Conversely,

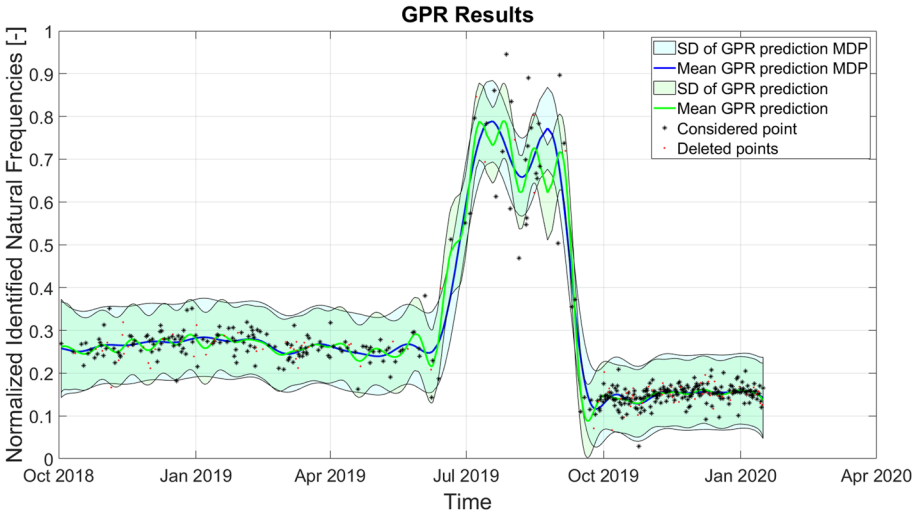

Fig. 8 Representation of the GPR prediction of Case 1 with MAR data points. The blue line is the mean value considering MD, the light blue area is the confidence interval bounded by the 5th and 95th percentile, the green line is the mean obtained in Case 0, the green area identifies the confidence interval of Case 0, the red dots represent omitted data points (randomly selected), finally, the black stars constitute the training dataset of remaining data points

the other two groups are well-defined, showcasing how the retrofitted structure has a generalised decrease in the first frequency w.r.t. to its pre-retrofitting configuration. Furthermore, in both clusters, the slight downward slope indicates the softening effects of increasing temperature in structural steel, as expected. In any case, the imputed values compare well with the other data and fall inside these clusters, thus enabling reliable modal tracking and cluster-based damage assessment.

4.2 Results of Case 1

To define the dataset used in Case 1, one-quarter of the data points, randomly selected among the ones left in the initial dataset (the one used in Case 0), were removed. Hence, the time series was reduced to 75% of its data points, corresponding to a training dataset of 357 elements. The GPR was thus applied to this dataset; its predictions are depicted in Fig. 8.

Even though the data points are reduced in the training dataset, the GPR-predicted interval confidence contains most of the identified natural frequencies. In addition, in the steady branches, the mean and the SD identified in Case 0 and Case 1 are similar, tending to overlap. Between July and September 2019, the two predictions become more dissimilar, with non-negligible differences in the predicted mean and standard deviation, which is caused by the combination of more fluctuating data and less dense data available. The overall performance predictions are extraordinary, as shown in Fig. 9. The histogram shows the percentual difference between the predicted value and the natural frequency value of all the available data points. In 63.3% of cases, the prediction differs by more than $\pm 10\%$; in 15.8% and 15.9% of cases, it is bounded, respectively, between $(-30\%, -10\%)$ and $(+10\%, +30\%)$. Finally, in 98.4% of cases, the difference is lower than $\pm 50\%$.

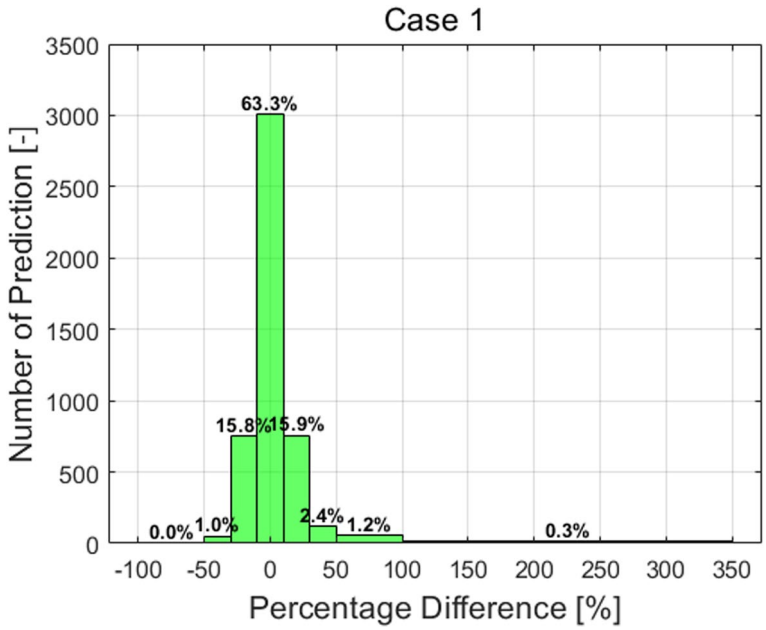

Fig. 9 Histogram representation of the percentage difference between the value of predicted frequencies and the value of corresponding identified natural frequencies

4.3 Results of Case 2

In this case, the initial dataset of Case 0 underwent the omission of n consecutive data points in arbitrary positions to investigate the effects of MNAR data points in more or less critical tracts of the non-stationary time series. Particularly:

- In Case 2.a, one hundred data points between the 350th and 450th positions have been omitted (corresponding to December 2019 and January 2020).
- Similarly, in Case 2.b, one hundred data points included between the 100th and 200th positions (corresponding to February and July 2019) have been manually removed.

For further investigation, the period between February and September 2019 has been further analysed with two shorter sections of MNAR data points:

- Case 2.c analyses the GPR performances when the omission occurs at the data between the 100th and 150th. (corresponding to February and March 2019)
- Case 2.d considers a data loss between the 200th and 220th positions (corresponding to August and November 2019).

In Cases 2.a and 2.b, the training dataset is reduced to 376 data points, which represents a 21% reduction of the training dataset with respect to Case 0. The results of prediction reliability are highly variable, depending on the stability of the data, the duration of data absence, and the temporal concentration of the data. The results of the GPR prediction are depicted in Fig. 10a and b.

For Case 2.a (Fig. 10a), the GPR prediction results along the signal are appreciable. Despite the data omission, the prediction results remain meaningful and reliable,

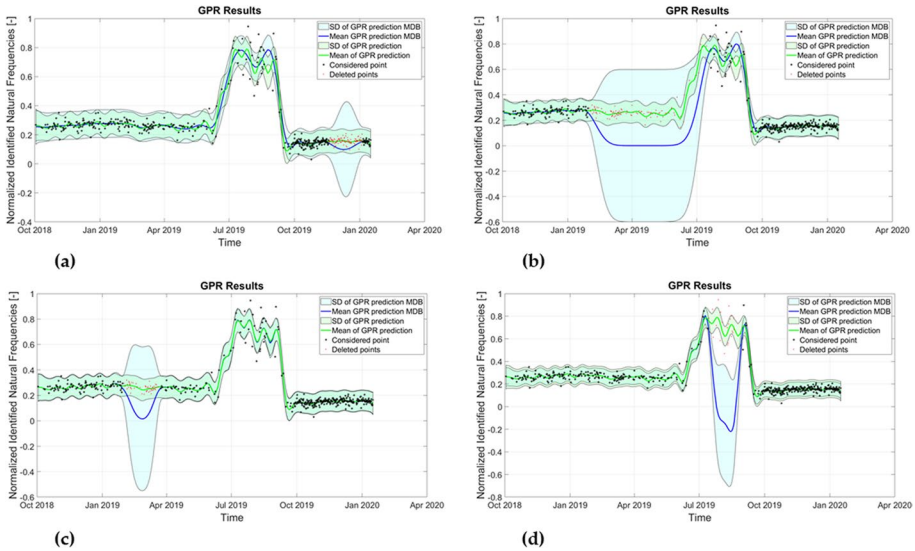

Fig. 10 Representation of the GPR prediction of the several variants of Case 2; in particular, (**a**) represents Case 2.a, while (**b**), (**c**) and (**d**) represent, in the same order, Case 2.b, Case 2.c and Case 2.d. The blue line is the mean value considering MD, the light blue area is the confidence interval bounded by the 5th and the 95th percentile with MD, the green line is the mean obtained in the Case 0, the green area identify the confidence interval of Case 0, the red dots represent omitted data point, finally the black star keys constitute the training dataset

although the confidence interval increases. Reasonably, the good results obtained during the process are due to the stable data before and after the omission, as well as the high density of available data. Figure 10b, associated with Case 2.b, demonstrates that the prediction results in the interval without data are speedily losing meaningfulness due to the high variability of the data given before and after the omission. The predicted mean function quickly trends toward zero, an outcome justifiable by the zero-mean assumption of GPR. It is interesting to note that in the range before and after the omitted data point, the prediction for this case resembles that of Case 0, where both the mean and the standard deviation tend to overlap those of the benchmark. That is to say, the GP regression is only locally affected by these time-limited issues with the measured data. Hence, in similar cases, the deleterious effects are very limited, moving farther from the affected tracts (i.e., for previous or later identifications). To mitigate this issue, integrating physical models and external covariates may lead to better results. For instance, temperature data - readily available from the same monitoring system - can be incorporated as an external covariate in the GPR model. Since ambient temperature has a well-documented influence on natural frequencies (e.g., softening of structural steel at higher temperatures (Farrar C. R. et al. 1994; Ding & Li 2011)), it can provide physical context during prolonged missing data intervals. As a proof of concept, one could leverage the known correlation between frequency and temperature – see e.g. Fig. 7c, where the tract of interest (pre-retrofit) corresponds to the area circled in red – to guide the GPR in extended MNAR gaps. This integration could take the form of a multi-variable GPR (Saida et al. 2024), where both time and temperature inform the covariance function, improving the reliability of long-gap imputation under non-stationary conditions. These possible solutions will be further investigated in future works.

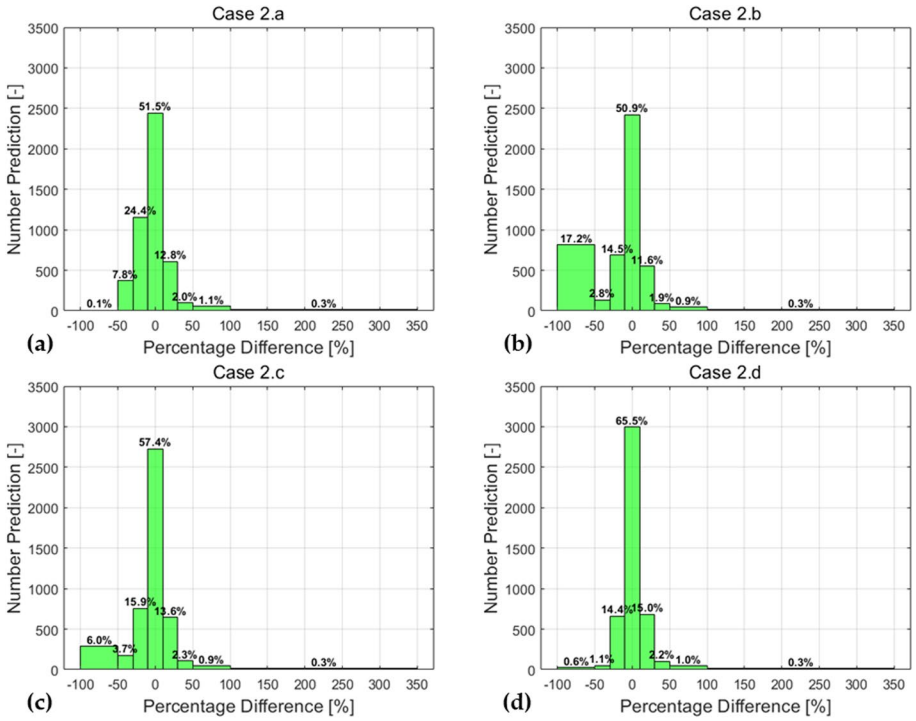

Fig. 11 Histogram representation of the percentage difference between the value of predicted frequencies and the value of corresponding identified natural frequencies. (**a**), (**b**), (**c**) and (**d**) represent, in the same order, Cases 2.a, 2.b, 2.c and 2.d

Figure 11a and b illustrate the percentage difference between the predicted and the identified natural frequencies in Cases 2.a and 2.b. In Case 2.a, 51.5% of the predictions differ by ±10%, while 24.4% and 12.8% of cases show differences ranging from −30% to −10% and +10% to +30%, respectively. In this case, 98.5% of predictions have a difference of less than ±50%. Compared with the results obtained in Case 0 and Case 1, the percentage of data predicted with a precision of ±10% has a significant reduction (more than 10 percentage points), which is redistributed among the other ranges, bounded between (-50%, -10%) and (+10%, +50%).

On the other hand, for Case 2.b, a conspicuous number of predictions (17.2%) differ from the actual data in the range bounded between (−100%, −50%). Conversely, 50.9% of the predictions differ by ≤±10%, while in 14.5% and 11.6% of cases, the difference ranges from −30% to −10% and +10% to +30%, in the same order. Thus, in this case, only 81.7% of predictions have a variance of less than ±50%. Hence, as highlighted by this Case 2.b, the omission of data for an extended period, coupled with data scarcity and high data variability, entails an abrupt decrease in the reliability of GPR prediction performances. For these reasons, additional analyses have been performed in this range.

Case 2.c is obtained by omitting the data between the 100th and 150th positions. The corresponding prediction is illustrated in Fig. 10c. The accuracy prediction quickly loses reliability in terms of both mean and standard deviation. Nevertheless, since the omission period is brief, the prediction returns rapidly to a good fit until it overlaps again with the one obtained in Case 0. Considering the precision obtained, depicted in Fig. 11c, 57.4% of predictions differ by ±10%, with 15.9% of cases ranging from −30% to

−10% and 13.6% of them included in (+10%, +30%). In this instance, 92.9% of predictions have a difference of less than ±50%.

Finally, as mentioned, Case 2.d is obtained by removing the data from the 200th and 220th positions. The corresponding prediction is depicted in Fig. 10d. The omission occurs during the period when the higher variability of identified natural frequencies is observed (July and October 2019). The prediction results are similar to those of Case 0 before and after the removal; however, in the proximity of the removal, they rapidly become not truly representative of the actual identified frequencies. In Fig. 11d, the precision reached by the GPR prediction is depicted. The histogram exhibits a good level of precision, almost equal to that obtained in Case 0; however, this interpretation is misleading. Indeed, the omission is performed on a restrained range, both in number and in time, and the loss of meaningfulness occurs only in the proximity of omitted data. In this way, relatively few predicted data points differ from the identified natural frequencies, but this difference is not negligible.

Considering the overall results, the goodness depends on the density of the data available before and after the omission, the stability of the data, and the length of the period during which the omission occurs. For example, in Cases 2.a and 2.c, where the data point density is high, the imputed values of the missing data points are stable, and the period is short, the results are significantly good. On the other hand, in Case 2.b, the results are meaningless in the range where the omission occurred, as the corresponding time period is longer and the data are sparse and highly variable. In Case 2.d, despite the short period, the high variability of the relatively scarce data renders the results quite meaningless.

5 Discussion and conclusions

This research work addressed missing data imputation in ordered time series of identified natural frequencies, considering both punctual MAR and prolonged MNAR gaps in the time histories. In particular, the use of Gaussian Process Regression (GPR) has been proposed for this aim.

To investigate the GPR performance within the intended scope, this case study utilises the identified natural frequencies of the KW51 steel tied-arch railway bridge for experimental validation. In particular, the period between October 2018 and January 2020 has been used since it includes a temporary variation of the natural frequencies due to structural retrofitting works. The initial dataset was obtained from the identifications of the first mode in these three phases (before, during, and after retrofitting). The GPR was trained on this dataset (Case 0) and on its manipulations with intentionally omitted data (Cases 1 and 2.a-2.d). Additionally, to assess the effectiveness of the presented methodology, the GPR results of Case 0 were compared with other uncertainty estimation approaches, such as mean imputation and linear regression. Furthermore, the method was tested on temperature recordings to examine its flexibility to different types of data.

More in detail, the analysis investigated three main cases: Case 0, in which the GPR was trained on the complete subsampled dataset; Case 1, obtained from the dataset of Case 0 by omitting one-fourth of the original data points (randomly selected from all the ones available in Case 0); and Case 2, obtained from Case 0 by omitting n consecutive data points. Case 2 was divided into four subcases: Case 2.a, Case 2.b, Case 2.c, and Case

2.d. These were obtained by omitting from the 350th to the 450th, from 100th to the 200th, from 100th to the 150th, and from the 200th to the 220th data point respectively.

Case 0 is intended as a reference in which other uncertainty estimation methods (mean imputation and linear regression) have been tested, comparing their results with the GPR ones. On the other hand, the instances represented in Case 1 and the several variants of Case 2 mimic different situations that can result from a malfunctioning of the monitoring system. Case 1 depicts a situation in which data points are occasionally missing, and the variants of Case 2 represent a more prolonged dysfunction, studying the effects at different tracts of the non-stationary signal.

From all these studies, it has been found that the reliability of the prediction performances is case-sensitive. In Case 0, this is outstanding: the utmost majority of the identified frequencies are included in the interval of confidence defined by GPR. In Case 1, when comparing the target value to the predicted one, precision is significant, as 98.4% of the imputed data points fall within the ±50% interval. Hence, from Case 1, it is possible to state that the effect of an occasional sensor misfunction does not significantly affect GPR prediction, thus proving the total feasibility of imputing MAR data points.

Meanwhile, in the case of a prolonged malfunction, the results of the prediction depend strongly on three different factors: the stationarity of the data, the duration of the dysfunction, and the density of the available data. In general, the prediction performance suffers a generalised decrease, thus highlighting some limitations for the direct use in case of MNAR data points, especially for non-stationary datasets such as the one used here. In fact, all the tests highlight how the GPR, which relies on a default constant value for its mean, struggles to adapt to prolonged missing data at critical moments, reverting back to that default value (here, zero).

In fact, Case 2.a exhibits only a slight performance decrease due to the short time duration, data stationarity in the tract of interest, and high data point density. In contrast, Case 2.b has all the factors working against it (low density, high non-stationarity, and longer duration), resulting in poor prediction performance. In Case 2.c, since the data are stationary and the time duration of misoperation is short, but the data are not particularly dense, the results achieved are considerable but inferior to those of Case 0. In Case 2.d, in which the time period is short but the data are scarce and volatile, the results are not extraordinarily meaningful.

Finally, regarding the comparison with the other common estimation approaches, the GPR significantly outperforms the mean imputation method, as it can manage non-stationary data, and exceeds linear interpolation, which fails to account for the statistical probability distribution of the predicted data. Additionally, to illustrate its adaptability, the GPR has been further tested on temperature measurements rather than identified natural frequencies, achieving satisfactory results again.

As a final thought, the analyses reported in this study were based on a purely data-driven approach, akin to a black box. The performance could be enhanced by exploiting the concept of the grey box models, in which the data-driven approach is combined with the physics-based one. This, especially in MNAR cases, where n consecutive data points are omitted (Case 2.a-2.d), could significantly improve the performance. Alternatively, the GPR can be combined with different sources of input data (e.g., from environmental monitoring), and/or other AI strategies to enhance its performance, especially to

account for the non-stationary effects. As diffusely discussed throughout the article, all these aspects will be addressed in future research works, focusing on integrating ML-based data imputation techniques directly into the damage assessment process.

Acknowledgements
The authors would like to thank the research group of Kristof Maes, Geert Lombaert, and their colleagues from KU Leuven for making the KW51 dataset publicly available.

Authors' contributions
Conceptualisation: M.C., V.D.B., B.C.; Methodology: M.D., M.C., V.D.B.; Software: M.D.; Validation: M.C.; Resources: V.D.B., B.C.; Data Curation: M.C.; Writing—Original Draft: M.D. and M.C.; Writing—Review & Editing: V.D.B. and B.C.; Visualisation: M.D. and M.C.; Supervision: M.C., V.D.B., B.C.; Project administration: B.C.; Funding acquisition: B.C.

Funding
This work is part of the research activity developed by the authors within the framework of the "PNRR": MOST – Sustainable Mobility National Research Center - SPOKE 7 "Cooperative Connected and Automated Mobility and Smart Infrastructures" - WP4"and received funding from the European Union Next-GenerationEU (PIANO NAZIONALE DI RIPRESA E RESILIENZA (PNRR) – MISSIONE 4 COMPONENTE 2, INVESTIMENTO 1.4 – D.D. 1033 17/06/2022).

Data availability
The publicly archived dataset analysed in this study is available, thanks to Kristof Maes, Geert Lombaert, and their colleagues from KU Leuven, at the link: https://zenodo.org/record/3745914.

Declarations

Competing interests
The authors declare that they have no competing interests.

Received: 27 December 2024 Accepted: 16 April 2025
Published online: 23 June 2025

References

1994–2024 The MathWorks, I. (n.d.). Gaussian Process Regression Models. https://It.Mathworks.Com/Help/Stats/Gaussian-Process-Regression-Models.Html.
Al-Ghalib AA, Mahmoud SM (2023) Structural Condition Classification of Railway Bridge KW51 Before, During, and After Retrofitting. Ce/papers 6(5):840–847. https://doi.org/10.1002/cepa.2073
Anastasopoulos, D. (2020). Structural health monitoring based on operational modal analysis from long gauge dynamic strain measurements. KU Leuven.
Anastasopoulos D, Maes K, De Roeck G, Lombaert G, Reynders EPB (2023) Structural health monitoring of the KW51 bridge based on detailed strain mode shapes: Environmental influences versus simulated damage. In Life-Cycle of Structures and Infrastructure Systems (pp. 391–398). CRC Press. https://doi.org/10.1201/9781003323020-45
Assolie A (2024) Advanced modeling techniques using hierarchical gaussian process regression in civil engineering. Asian Journal of Civil Engineering 25(7):5599–5612. https://doi.org/10.1007/s42107-024-01132-7
Rasmussen C E, & Nickisch H, (2020, July 14). Documentation for GPML Matlab Code version 4.2. https://Gaussianprocess.Org/Gpml/Code/Matlab/Doc/-Last. Access 15/09/2024
Civera M, Boscato G, Zanotti Fragonara L (2020) Treed gaussian process for manufacturing imperfection identification of pultruded GFRP thin-walled profile. Compos Struct 254:112882. https://doi.org/10.1016/j.compstruct.2020.112882
Civera M, Surace C (2021) A Comparative Analysis of Signal Decomposition Techniques for Structural Health Monitoring on an Experimental Benchmark. Sensors 21(5):1825. https://doi.org/10.3390/s21051825
Civera M, Surace C, Worden K (2017) Detection of Cracks in Beams Using Treed Gaussian Processes (pp. 85–97). https://doi.org/10.1007/978-3-319-54109-9_10
Cross EJ, Manson G, Worden K, Pierce SG (2012) Features for damage detection with insensitivity to environmental and operational variations. Proceedings of the Royal Society a: Mathematical, Physical and Engineering Sciences 468(2148):4098–4122. https://doi.org/10.1098/rspa.2012.0031
Cross EJ, Worden K, Chen Q (2011) Cointegration: a novel approach for the removal of environmental trends in structural health monitoring data. Proceedings of the Royal Society a: Mathematical, Physical and Engineering Sciences 467(2133):2712–2732. https://doi.org/10.1098/rspa.2011.0023
Daniels MJ, Hogan JW (2008) Missing Data in Longitudinal Studies. Chapman and Hall/CRC. https://doi.org/10.1201/9781420011180
Ding Y, Li A (2011) Temperature-induced variations of measured modal frequencies of steel box girder for a long-span suspension bridge. International Journal of Steel Structures 11(2):145–155. https://doi.org/10.1007/s13296-011-2004-4
Emmanuel T, Maupong T, Mpoeleng D, Semong T, Mphago B, Tabona O (2021) A survey on missing data in machine learning. J. Big Data, 8(1). https://doi.org/10.1186/s40537-021-00516-9
Erler NS, Rizopoulos D, van Rosmalen J, Jaddoe VWV, Franco OH, Lesaffre EMEH (2016) Dealing with missing covariates in epidemiologic studies: a comparison between multiple imputation and a full Bayesian approach. Stat Med 35(17):2955–2974. https://doi.org/10.1002/sim.6944

Farrar CR, Baker WE, Bell TM, Cone KM, Darling TW, Duffey TA, Eklund A, Migliori A (1994) Dynamic Characterization and Damage Detection in the I-40 Bridge Over the Rio Grande.
Faruqi MA, Roy S, Salem A (2012) Elevated temperature deflection behavior of concrete members reinforced with FRP bars. https://doi.org/10.1177/1042391512447045, 22(3), 183–196. https://doi.org/10.1177/1042391512447045
Hoang N-D, Pham A-D, Nguyen Q-L, Pham Q-N (2016) Estimating Compressive Strength of High Performance Concrete with Gaussian Process Regression Model. Advances in Civil Engineering 2016:1–8. https://doi.org/10.1155/2016/2861380
Ibrahim JG, Chen M-H, Lipsitz SR, Herring AH (2005) Missing-Data Methods for Generalized Linear Models. J Am Stat Assoc 100(469):332–346. https://doi.org/10.1198/016214504000001844
Jie Wang (2024) An Intuitive Tutorial to Gaussian Process Regression. Computing in Science & Engineering.
Kim D, Kim D-Y, Ko T, Hwan Lee S (2024) Physics-informed Gaussian process regression model for predicting the fatigue life of welded joints. International Journal of Fatigue, 108644. https://doi.org/10.1016/j.ijfatigue.2024.108644
Lin WC, Tsai CF (2020) Missing value imputation: a review and analysis of the literature (2006–2017). Artif Intell Rev 53(2):1487–1509. https://doi.org/10.1007/s10462-019-09709-4
Luo Y (2022) Evaluating the state of the art in missing data imputation for clinical data. Brief. Bioinforma., 23(1), bbab489. https://doi.org/10.1093/bib/bbab489
Ma Z, Chen G (2018) Bayesian methods for dealing with missing data problems. Journal of the Korean Statistical Society 47(3):297–313. https://doi.org/10.1016/j.jkss.2018.03.002
Maes K, Lombaert G (2021) Monitoring Railway Bridge KW51 Before, During, and After Retrofitting. Journal of Bridge Engineering, 26(3). https://doi.org/10.1061/(ASCE)BE.1943-5592.0001668
Maes K, Van Meerbeeck L, Reynders EPB, Lombaert G (2022) Validation of vibration-based structural health monitoring on retrofitted railway bridge KW51. Mech Syst Signal Process 165:108380. https://doi.org/10.1016/j.ymssp.2021.108380
Mason A, Best N, Plewis I, Richardson S (2010a) Insights into the use of Bayesian models for informative missing data. In *Technical report*. Imperial College.
Mason A, Richardson S, Plewis I, Best N (2010b) Strategy for modelling non-random missing data mechanisms in observational studies using Bayesian methods. *Technical Report*.
Omidinasab F, Sahraei Moghadam A, Dowlatshahi MB (2023) Predictive model for shear strength estimation in reinforced concrete beams with recycled aggregates using Gaussian process regression. Neural Comput Appl 35(11):8487–8503. https://doi.org/10.1007/s00521-022-08126-z
Pal M, Deswal S (2010) Modelling pile capacity using Gaussian process regression. Comput Geotech 37(7–8):942–947. https://doi.org/10.1016/j.compgeo.2010.07.012
Pozzi M, Wang Q (2018) Gaussian Process Regression and Classification for Probabilistic Damage Assessment of Spatially Distributed Systems. KSCE J Civ Eng 22(3):1016–1026. https://doi.org/10.1007/s12205-018-0014-x
Rasmussen CE (2004) Gaussian Processes in Machine Learning (pp. 63–71). https://doi.org/10.1007/978-3-540-28650-9_4
Rasmussen CE, De HM (2010) Gaussian Processes for Machine Learning (GPML) Toolbox Hannes Nickisch. Journal of Machine Learning Research, 11, 3011–3015. http://www.kyb.tuebingen.mpg.de/bs/people/carl/code/minimize/.
Roy S, Unobe I, Sorensen AD (2021) Vehicle-Impact Damage of Reinforced Concrete Bridge Piers: A State-of-the Art Review. J Perform Constr Facil 35(5):03121001. https://doi.org/10.1061/(ASCE)CF.1943-5509.0001613/ASSET/C6794735-D982-4821-ADCD-95D654D158E5
Saida T, Rashid M, Nishio M (2024) System fragility analysis of highway bridge using multi-output Gaussian process regression surrogate model. Adv Struct Eng 27(16):2803–2822. https://doi.org/10.1177/13694332241291255
Samui P, Jagan J (2013) Determination of effective stress parameter of unsaturated soils: A Gaussian process regression approach. Front Struct Civ Eng 7(2):133–136. https://doi.org/10.1007/s11709-013-0202-1
Shadbahr T, Roberts M, Stanczuk J, Gilbey J, Teare P, Dittmer S, Thorpe M, Torné RV, Sala E, Lió P, Patel M, Preller J, Selby I, Breger A, Weir-McCall JR, Gkrania-Klotsas E, Korhonen A, Jefferson E, Langs G, … Schönlieb C-B (2023) The impact of imputation quality on machine learning classifiers for datasets with missing values. *Communications Medicine 2023 3:1*, *3*(1), 1–15. https://doi.org/10.1038/s43856-023-00356-z
Sohn H (2007) Effects of environmental and operational variability on structural health monitoring. Philosophical Transactions of the Royal Society a: Mathematical, Physical and Engineering Sciences 365(1851):539–560. https://doi.org/10.1098/rsta.2006.1935
Tsuda Y, Tomizawa Y, Yoshida I, Wada M, Suemasa N, Otake Y (2023) Estimation of engineering bedrock layer utilizing ground surface elevation in Gaussian process regression. Comput Geotech 160:105548. https://doi.org/10.1016/j.compgeo.2023.105548
van de Velde M, Maes K, Lombaert G (2023) Modelling the Nonlinear Behavior of the Pot Bearings of Railway Bridge KW51. Journal of Bridge Engineering, 28(6). https://doi.org/10.1061/JBENF2.BEENG-6144
Worden K, Becker WE, Rogers TJ, Cross EJ (2018) On the confidence bounds of Gaussian process NARX models and their higher-order frequency response functions. Mech Syst Signal Process 104:188–223. https://doi.org/10.1016/j.ymssp.2017.09.032
Worden K, Surace C, Becker W (2017) Uncertainty Bounds on Higher-Order FRFs from Gaussian Process NARX Models. Procedia Engineering 199:1994–2000. https://doi.org/10.1016/j.proeng.2017.09.317
Wu X, Yang F, Huang S (2024) Predicting CBR values using gaussian process regression and meta-heuristic algorithms in geotechnical engineering. Multiscale and Multidisciplinary Modeling, Experiments and Design 7(4):3799–3813. https://doi.org/10.1007/s41939-024-00428-0

Publisher's Note